MedChemComm

RESEARCH ARTICLE

View Article Online
View Journal

Cite this: DOI: 10.1039/c6md00406g

Discovery of cyclopropyl chromane-derived pyridopyrazine-1,6-dione γ-secretase modulators with robust central efficacy†

Martin Pettersson,*[a] Douglas S. Johnson,[a] Danica A. Rankic,*[d] Gregory W. Kauffman,[a] Christopher W. am Ende,[d] Todd W. Butler,[d] Brian Boscoe,[d] Edelweiss Evrard,[a] Christopher J. Helal,[d] John M. Humphrey,[d] Antonia F. Stepan,[a] Cory M. Stiff,[d] Eddie Yang,[d] Longfei Xie,[d] Kelly R. Bales,[b] Eva Hajos-Korcsok,[b] Stephen Jenkinson,[g] Betty Pettersen,[f] Leslie R. Pustilnik,[e] David S. Ramirez,[g] Stefanus J. Steyn,[c] Kathleen M. Wood[b] and Patrick R. Verhoest[a]

Received 18th July 2016,
Accepted 5th October 2016

DOI: 10.1039/c6md00406g

www.rsc.org/medchemcomm

Herein we describe the discovery of a novel series of cyclopropyl chromane-derived pyridopyrazine-1,6-dione γ-secretase modulators for the treatment of Alzheimer's disease (AD). Using ligand-based design tactics such as conformational analysis and molecular modeling, a cyclopropyl chromane unit was identified as a suitable heterocyclic replacement for a naphthyl moiety that was present in the preliminary lead **4**. The optimized lead molecule **44** achieved good central exposure resulting in robust and sustained reduction of brain amyloid-β42 (Aβ42) when dosed orally at 10 mg kg^{-1} in a rat time-course study. Application of the unpaced isolated heart Langendorff model enabled efficient differentiation of compounds with respect to cardiovascular safety, highlighting how minor structural changes can greatly impact the safety profile within a series of compounds.

Introduction

Alzheimer's disease (AD) is the most common form of dementia among the elderly population, affecting approximately 1 in 5 people over the age of 65.[1] It is a debilitating neurodegenerative disease that presents with gradual loss of memory, impaired speech, inability to carry out tasks of daily living, and is ultimately fatal.[1] AD pathology is characterized by the accumulation of amyloid plaques consisting primarily of Aβ42, which is a neurotoxic peptide produced *via* sequential processing of the amyloid precursor protein (APP) by the β-secretase (BACE) and γ-secretase enzymes. In an effort to develop disease-modifying therapies that can slow or halt the progression of AD, inhibition or modulation of these enzymes has been aggressively pursued to reduce formation of Aβ42.[2]

γ-Secretase modulators (GSMs) have emerged as a promising therapeutic approach for AD.[3,4] This class of compounds has a mechanism of action that is distinct from that of γ-secretase inhibitors (GSIs). While GSIs inhibit processing of all γ-secretase substrates including notch, which is critical for normal cell signaling, GSMs alter the cleavage site of APP to reduce formation of longer, aggregation-prone peptides in favor of shorter, more benign species. Data suggests that Aβ40, which is present at ~10 times the concentration of Aβ42 in a healthy human brain, can sequester Aβ42 in stable mixed tetramers, potentially preventing further oligomerization of Aβ42.[5] GSMs therefore hold the promise of selectively reducing levels of the toxic species without inhibiting notch signaling, and avoiding the side effects observed in GSI clinical trials.[6,7] γ-Secretase is comprised of four subunits: presenilin, Aph-1, nicastrin, and Pen-2.[8] Chemical biology studies using photoaffinity probes have established that GSMs bind to allosteric sites on presenilin that are different from those targeted by GSIs.[9,10]

Analysis of the GSM literature clearly reveals the challenge of identifying potent GSMs within favorable CNS physicochemical property space.[11] γ-Secretase is an intra-membrane

[a] *Neuroscience and Pain Medicinal Chemistry, Cambridge, Massachusetts 02139, USA. E-mail: martin.pettersson@pfizer.com; Tel: +(617) 395 0705*
[b] *Neuroscience and Pain Research Unit, Cambridge, Massachusetts 02139, USA*
[c] *Pharmacokinetics, Dynamics and Metabolism, Pfizer Worldwide Research and Development, Cambridge, Massachusetts 02139, USA*
[d] *Neuroscience and Pain Medicinal Chemistry, Groton, Connecticut 06340, USA. E-mail: danica.rankic@pfizer.com; Tel: +(860) 441 4354*
[e] *Primary Pharmacology Group, Groton, Connecticut 06340, USA*
[f] *Drug Safety R&D, Pfizer Worldwide Research and Development, Groton, Connecticut 06340, USA*
[g] *Global Safety Pharmacology, Pfizer Worldwide Research and Development, La Jolla, California 92121, USA*

† Electronic supplementary information (ESI) available. CCDC 1452774. For ESI and crystallographic data in CIF or other electronic format see DOI: 10.1039/c6md00406g

cleaving aspartyl protease, which may underlie the apparent requirement for compounds to have increased lipophilicity in order to achieve robust potency.[12] Our initial efforts led to the discovery of dihydrobenzofuran amide GSMs as exemplified by **1** (Scheme 1).[13,14] Because of difficulties in further improving potency while maintaining acceptable physicochemical properties and ADME (absorption, distribution, metabolism, and excretion) characteristics, we shifted our efforts toward the design of novel, conformationally restricted heterocyclic cores with increased polarity. As previously described, this led to the discovery of the pyridopyrazine-1,6-dione series (*e.g.*, **2** and **3**), which had several advantages such as improved potency, good metabolic stability, low MDR efflux ratio, and reduced inhibition of cyctochrome P450 (CYP450) enzymes.[15,16] During this time, the team had also identified naphthyl derivative **4**, which had one of the highest ligand efficiency values (LE = 0.34) thus far, and it was therefore selected for further optimization (Scheme 1). A rapid survey of diverse chemical space using parallel medicinal chemistry (PMC) led to identification of an indole as a suitable heterocyclic replacement for the naphthyl moiety.[17,18] Further optimization eventually delivered **5**, which was a highly potent modulator of γ-secretase *in vitro* in Chinese hamster ovary cells overexpressing wild-type human APP (CHO APP) (Aβ42 IC_{50} = 6 nM, clog*P* = 3.1).[19] However, poor central Aβ42-lowering activity was observed with this compound in an acute *in vivo* efficacy study in rat (in part due to reduced central exposure), prompting further investigation into alternative heterocyclic replacements for the naphthyl group.[17] Herein we describe the design and synthesis leading to the discovery of cyclopropyl chromane-derived GSMs, which overcame significant safety hurdles and achieved excellent Aβ42-lowering activity *in vivo*.

Results and discussion

Given the poor exposure and efficacy of the indole series, we envisioned that a chromene might serve as a more suitable replacement for the naphthyl unit. Chromenes feature prominently in bioactive natural products, and incorporation of this ring system would result in reduced aromatic ring-count and increased polarity while avoiding the addition of basic centers that could serve as recognition elements for P-glycoprotein (P-gp)-mediated efflux. Several synthetic routes were developed to facilitate efficient evaluation of structure–activity relationships (SAR). Our general strategy involved the use of lactone **7** as a common starting material[17] in combination with a variety of chromene-derived amines **8** (Scheme 2). We envisioned that the chromene motif could be accessed from an intramolecular hydroarylation/amination sequence. The substrate required for the hydroarylation chemistry could be derived from readily available starting materials such as appropriately substituted phenols and alkynes. Given that a large number of substituted phenol monomers are readily available, this strategy would enable facile evaluation of the chromene SAR.

4-(Trifluoromethyl)phenol (**12**) was alkylated with propargyl bromide (**11**, Scheme 3). The resultant alkynyl arene **13** was deprotonated and then reacted with paraformaldehyde to install the hydroxymethyl moiety. Cyclization of **14** to generate the chromene ring system **15** was initially performed using indium triiodide.[20] The primary alcohol of **15** was then converted to the amine **16** *via* a two-step process involving Mitsunobu reaction with phthalimide followed by hydrazine-mediated deprotection. The corresponding saturated chromane amine **17** was readily accessed *via* hydrogenation of **16**. The chromene/chromane amines **16** and **17**

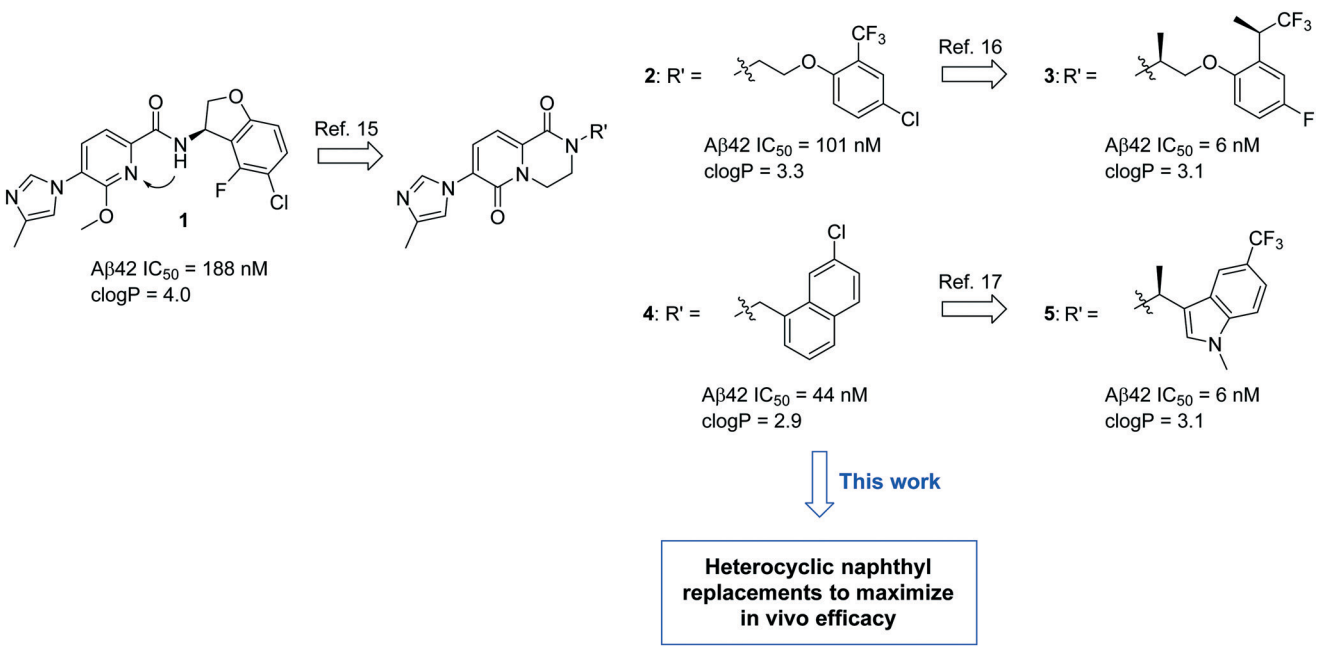

Scheme 1 Design of pyridopyrazine-1,6-dione GSMs.

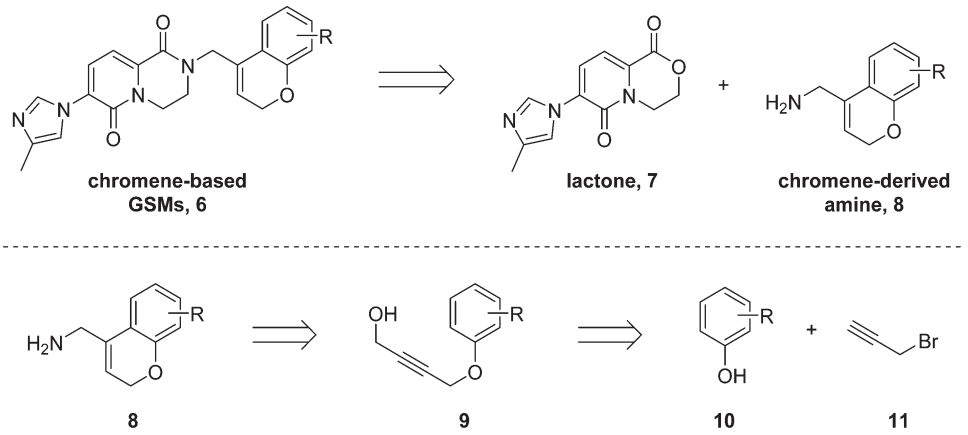

Scheme 2 Overview of synthetic strategy.

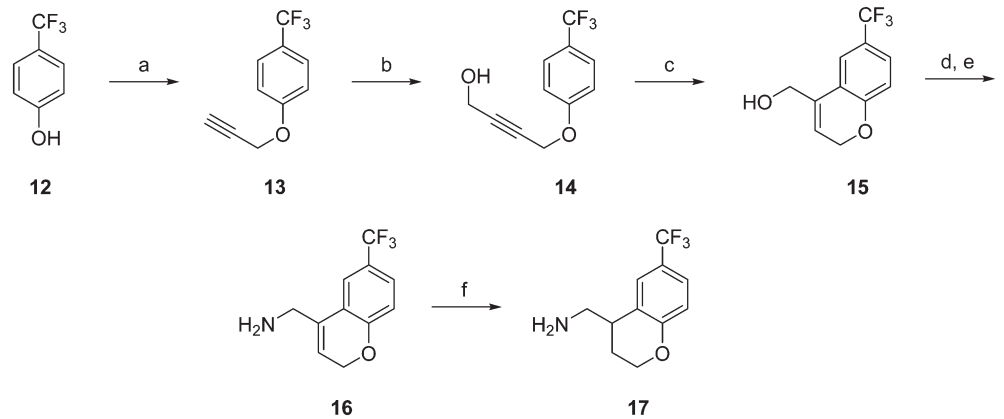

Scheme 3 Synthesis of chromene amine **16** and chromane amine **17**. Reagents and conditions: (a) propargyl bromide, K_2CO_3, DMF, quantitative; (b) *n*-BuLi, −78 °C then paraformaldehyde, 56%; (c) InI_3, THF, 73%; (d) phthalimide, DIAD, PPh_3, 58%; (e) hydrazine hydrate, 57%; (f) Pd/C, 40 psi H_2, 88%.

were then coupled to lactone **7** *via* a DABCO bis-trimethylaluminum (DABAL-Me_3)-mediated amidation to afford **18** and **19** (Scheme 4),[17] whereupon cyclization to the pyridopyrazine-1,6-dione core could be accomplished *via in situ* activation of the primary alcohol as the mesylate, followed by intramolecular alkylation to afford **20** and **21**. Note that low yields were observed in the synthesis of compound **20** due to its susceptibility to air oxidation.

The hydroarylation strategy also proved valuable for the preparation of more sterically demanding chromene analogs. By simply varying the alkyne unit of the cyclization precursor, we were able to readily access *gem*-dimethyl propargyl alcohols such as **23** (Scheme 5). In this case, the subsequent cyclization was carried out using a gold-based catalyst.[21] It was found that protection of the free alcohol with a silyl group prior to cyclization provided extremely clean reaction profiles

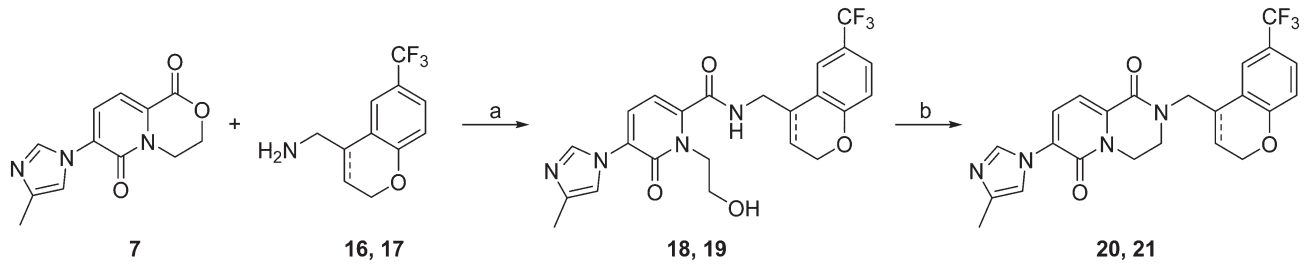

Scheme 4 Synthesis of chromene GSM **20** and chromane GSM **21**. Reagents and conditions: (a) DABAL-Me_3, THF, 40 °C; (b) Ms_2O, −20 °C then TBD, 28% over two steps for **20**, and PPh_3, DIAD, 57% over two steps for **21**.

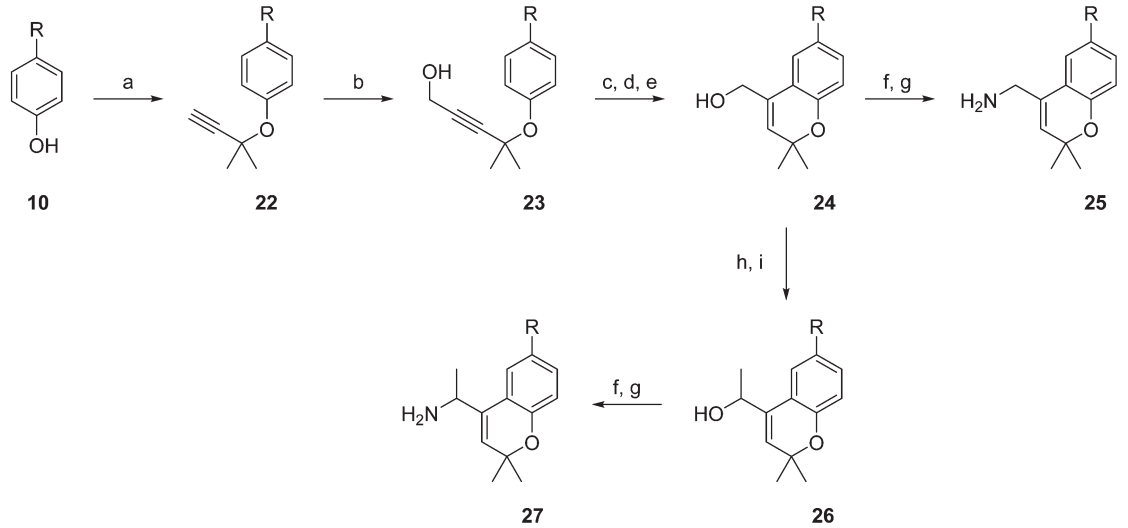

Scheme 5 Synthesis of *gem*-dimethyl-substituted amine intermediates **25** and **27**. Reagents and conditions: (a) 2-methyl-3-butyn-2-ol, TFAA, CuBr, −5 °C; (b) *n*-BuLi, −78 °C; then paraformaldehyde; (c) TBSCl, imidazole; (d) (JohnPhos)Au(MeCN)SbF_6 (1–5 mol%); (e) TBAF; (f) phthalimide, DIAD, PPh_3; (g) hydrazine hydrate (h) Dess–Martin periodinane; (i) MeMgBr, −78 °C to r.t. Note: R = Cl, CF_3, OCF_3; see Table 1 for details.

and high yields; however, protection was not necessary in all cases. Following cyclization and deprotection, the resultant allylic alcohol intermediates **24** could be converted to their corresponding amines **25** and then coupled to lactone **7** in a sequence similar to that shown in Scheme 4, affording *gem*-dimethyl-substituted chromene GSMs such as **28** and **29** (Table 1). Alternatively, oxidation of the allylic alcohol **24** to the corresponding aldehyde, followed by addition of methylmagnesium bromide, afforded secondary alcohol intermediate **26**. Mitsunobu reaction with phthalimide followed by hydrazine-mediated deprotection afforded amine **27**, which smoothly underwent lactam formation to afford alpha-methyl substituted GSMs **30–32**.

The initial chromene analog **20** exhibited an encouraging level of potency (Aβ42 IC_{50} = 30 nM, clog*P* = 2.4), but poor metabolic stability was observed in human liver microsomes (HLM $CL_{int,app}$ = 108 μL/min/kg).[22,23] This was not entirely surprising, as we suspected that the methylene between the olefin and the chromene oxygen may be susceptible to CYP-mediated oxidative metabolism. In fact, metabolite ID studies indicated that this site is indeed rapidly oxidized to afford the corresponding chromen-2-one. The related saturated chromane **21** (racemic) showed improved metabolic stability, but this structural modification resulted in a significant loss of potency. We therefore sought to block the site of metabolism on the chromene. Efforts to introduce *gem*-difluoro substitution were met with failure owing to instability of several of the synthetic intermediates. In fact, examples in the literature describing the synthesis of *gem*-difluorochromenes are very limited.[24] We therefore opted to block the metabolically labile site with *gem*-dimethyl substitution. Interestingly, the *gem*-dimethyl chromene moiety is commonly observed in natural products.[25] Although this modification would lead to an increase in log*P*, we hoped for an improvement in lipophilic metabolism efficiency (LipMetE).[26] Toward this end, **28** was prepared; the *gem*-dimethyl substitution was found to be well tolerated with respect to potency (Aβ42 IC_{50} = 13 nM). Although lipophilicity was increased from a clog*P* value of 2.4 to 3.4, metabolic stability was significantly improved ($CL_{int,app}$ values of 108 and 47.8 μL/min/mg for **20** and **28**, respectively), indeed generating an increase in LipMetE, from 0.6 to 1.3.

At this point, we observed that SAR trends from the indole series in many cases were applicable to the chromene series.[17] For example, replacing the critical trifluoromethyl substituent with a less lipophilic chlorine atom, as in **29**, led to a reduction in activity. Introduction of a conformational constraint *via* insertion of an (*S*)-methyl substituent on the methylene linker to afford **30** delivered an almost three-fold improvement in potency while maintaining good metabolic stability (Aβ42 IC_{50} = 4.9 nM, $CL_{int,app}$ = 14.3 μL/min/mg). In contrast, the enantiomer **31** was approximately 160-fold less active than **30**. Finally, a survey of alternative lipophilic, non-metabolizable replacements for the CF_3 substituent proved fruitful, with the trifluoromethoxy analogue **32** exhibiting a favorable profile (Aβ42 IC_{50} = 6.0 nM, $CL_{int,app}$ = 25.7 μL/min/mg). Notably, the two chromenes **30** and **32** maintained MDR ER values less than 2.0, suggesting a low risk for P-gp-mediated efflux.

An analysis of the aryl-imidazole GSM literature provides numerous examples of rigid and/or constrained analogues with excellent potency, suggesting that the orientation of the lipophilic group is rather well-defined in the active conformation, and that this substituent prefers to be oriented in a "turned" conformation below the plane of the core, as drawn in Fig. 1.[11] To understand the effect of the (*S*)-methyl substituent on conformation of the chromene series, we applied molecular modeling and conformational analysis to both **28** and **30** (see ESI† for details on the computational work-flow). The analysis revealed that the lowest energy

Table 1 *In vitro* pharmacology and disposition data for pyridopyrazine-1,6-dione GSMs **20**–**32**

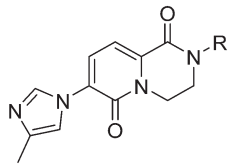

	R	IC_{50} (Aβ42, nM)[a]	clog *P*	MDR ER[b]	HLM $CL_{int,app}$ (μL/min/mg)[c]
20	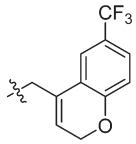	30	2.4	1.7	108
21	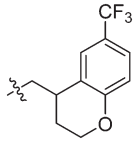	322	2.5	1.9	37.6
28	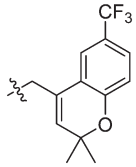	13	3.4	2.0	47.8
29	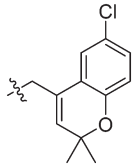	53	3.1	1.9	n.d.[d]
30	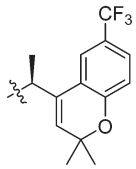	4.9	3.7	1.9	14.3
31	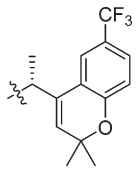	801	3.7	1.8	242
32	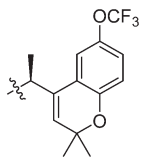	6.0	3.8	1.9	25.7

[a] Aβ42 IC_{50} values were obtained in a whole-cell assay using CHO APP_{wt} cells. Aβ42 IC_{50} values are the geometric mean of at least three experiments except for compound **20** (n = 2). [b] MDR efflux ratio using an MDR1/MDCK assay utilizing MDCK cells transfected with the gene that encodes human P-glycoprotein.[27] [c] Human liver microsome-derived intrinsic clearance.[22,23] [d] Not determined.

conformation of **28** does indeed prefer a "turned" conformation consistent with the putative bioactive conformation and conformationally restricted GSMs reported in the patent literature (Fig. 1a).[11] However, given the pseudo-symmetry above and below the planar pyridopyrazine core and the absence of a conformational control element, there are two possible conformers of equal probability (Fig. 1b). Consistent with our observations in the indole series,[17] introduction of the (*S*)-methyl substituent (**30**) reinforces the chromene group in the putative bioactive conformation, below the plane of the core, with a probability >99% (Fig. 1c). Conversely, modeling predicted that the (*R*)-methyl analogue **31** would be locked in the undesired conformation *above* the plane of the core. We hypothesize that this results in

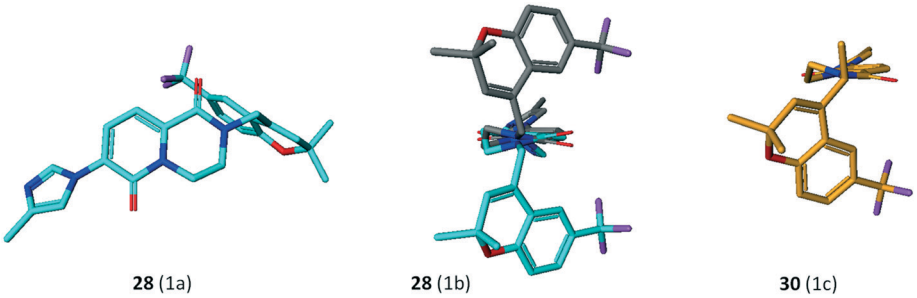

Fig. 1 a) The lowest energy conformer of **28** adopts a turned conformation that places the chromene moiety below the plane of the pyridopyrazine core; b) lacking a conformational control element, chromene **28** is expected to exist in a 1 : 1 ratio of two conformers; c) chromene **30**, bearing the (*S*)-methyl group, is predicted to exist primarily in a single conformer – the putative bioactive orientation.

the remarkable difference in potency between **30** and **31** (Table 1).

While exploring geminal dimethyl substitution on the chromene as a means of improving metabolic stability, an alternative approach was pursued in parallel. The key design objective was to identify additional heterocyclic systems that would force the terminal aryl ring to adopt the putative bioactive conformation. Analysis of compounds **20** and **21**, among other SAR trends, led us to conclude that sp^2 hybridization was required at the center connecting the methylene linker to the terminal heterocycle to achieve good Aβ42-lowering activity. With this in mind, we envisioned that the chromene olefin could be replaced with a cyclopropyl ring; we anticipated that this modification would both maintain sufficient sp^2 character and serve as an efficient conformational control element (Scheme 6). Application of the conformational analysis workflow described above to cyclopropyl chromane **33** supported this hypothesis, suggesting that this (*S*,*S*) diastereomer, with a 92% probability, would position the cyclopropyl chromane moiety in the requisite bioactive conformation, below the plane of the core (Fig. 2). Furthermore, we hypothesized that this design may lead to improved metabolic stability, as the resultant chromane methylene is no longer allylic.

The initial synthetic approach to cyclopropyl chromane-derived GSMs such as **33** relied on allylic alcohol intermediate **15** (Scheme 7). This material was subjected to a Simmons–Smith cyclopropanation to afford cyclopropyl alcohol **34**. A subsequent two-step alcohol-to-amine interconversion delivered **35**, which was then reacted with lactone **7** as previously described. The resulting racemic cyclopropyl chromane GSM (not shown) was separated *via* chiral HPLC to afford the enantiomerically pure analogs **33** and **40** (Table 2).

We quickly realized that routes relying on Simmons–Smith cyclopropanation of chromene alcohols such as **15** were not ideal as the cyclopropanation was not suitable for large-scale chemistry due to the safety concerns associated with diethylzinc. This problem was addressed by turning to the Corey–Chaykovsky cyclopropanation, a more benign and scalable method, to access the cyclopropyl chromane system. In order to generate the requisite α,β-unsaturated ester **37**, the synthetic sequence was modified slightly (Scheme 8). This route also accommodated installation of the *gem*-dimethyl substituents in analogy with chromene GSMs **28–32**. The ester moiety was installed by lithiation of the previously described alkynyl derivative **22**, followed by reaction with ethyl chloroformate to afford **36**, which in turn underwent gold-catalyzed cyclization to provide **37**. We were initially concerned that 1,4-addition of the Corey–Chaykovsky reagent might be impeded due to steric hindrance imparted by the *gem*-dimethyl substituents. However, the reaction proceeded smoothly to provide the corresponding cyclopropyl chromane intermediate in good yield. Subsequent reduction of the ester with DIBAL-H provided the alcohol **38**, which was then converted to amine **39**. The previously employed two-step process involving Mitsunobu reaction with phthalimide and deprotection with hydrazine was replaced with a more step- and atom-efficient one-pot process involving tosylation followed by displacement with ammonia to afford amine **39**. Finally,

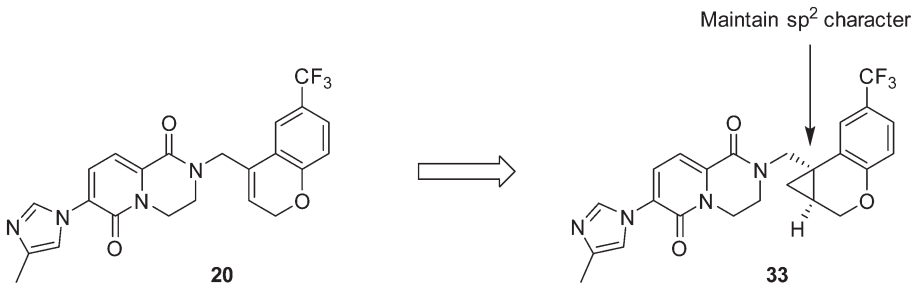

Scheme 6 Design of cyclopropyl chromane series.

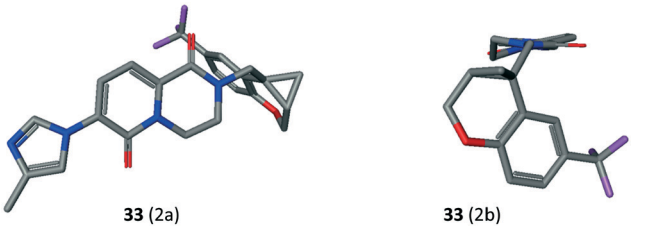

Fig. 2 Conformational analysis of cyclopropyl chromane **33** indicates that the desired bioactive orientation – below the plane of the core – is the predominant conformation. a) Extended view of **33**; b) end-to-end view of **33**.

condensation/cyclization with lactone **7** and chiral separation delivered the desired analogs such as **44** and **45** (Table 2).

The cyclopropyl chromane strategy actually led to an improvement in Aβ42-lowering activity, with **33** having an IC_{50} value of 5.6 nM, *versus* 30 nM for **20**. Notably, the opposite enantiomer **40** was 23-fold less potent. In accordance with the design objectives, metabolic stability of **33** was significantly improved compared to **20** (HLM $CL_{int,app}$ values of 37.9 and 108 μL/min/mg, respectively). Furthermore, cyclopropyl chromane **33** exhibited an MDR ER of less than 2.5 despite being one of our most polar GSMs under 10 nM made to date (clog P = 2.2, LipE = 5.0).[28] SAR of the cyclopropyl chromanes tracked very closely with both the chromene and the indole series. For example, CF_3-substitution in the 6-position was critical for potency: moving this substituent to the 7-position (*i.e.*, **41**) or replacing it with a methoxy group (**43**) led to significant loss in Aβ-lowering activity.

At this stage, cyclopropyl chromane **33** appeared to be the optimal compound based on its exquisite *in vitro* potency, improved metabolic stability, and reduced lipophilicity, and it was therefore selected for evaluation in a rat efficacy model. However, as seen with several earlier compounds such as **3** and **5**, poor central Aβ42-lowering activity was observed, which was attributed in part to inadequate central exposure (data not shown). The challenge of achieving robust central activity with γ-secretase modulators of reduced lipophilicity has been well documented in the literature.[11,12] We therefore hypothesized that the *in vitro*/*in vivo* disconnect observed with **33** potentially could be rescued by a slight increase in lipophilicity. Taking a cue from the chromene series, we therefore installed *gem*-dimethyl substitution on the cyclopropyl chromane methylene. Gratifyingly, this structural modification had little impact on potency, and **44** maintained acceptable metabolic stability and MDR ER, with Aβ42 IC_{50} = 4.9 nM, $CL_{int,app}$ = 34.5 μL/min/mg, and MDR ER = 2.5. Likewise, the corresponding trifluoromethoxy substituted compound **45** was equipotent with a similar ADME profile.

At this juncture, chromenes **30** and **32** and cyclopropyl chromanes **44** and **45** were selected for in-depth profiling *in vivo* based on their superior *in vitro* potency and favorable ADME profile. However, lethality was observed with chromene **30** at 40 mg kg^{-1} in a rat time-course efficacy study, whereas cyclopropyl chromanes **44** and **45** were well tolerated at the same dose. Given that this unexpected adverse event, which was confirmed in a rat dose-escalation study (*vide infra*), appeared rapidly and seemed to be C_{max}-driven, we hypothesized that it could be attributed to an acute cardiovascular (CV) safety liability. To test this hypothesis, we turned to the use of the rat unpaced isolated heart Langendorff assay, which allows measurement of left ventricle pressure/contractility, heart rate, and coronary vascular perfusion pressure.[29,30] This model can help determine whether there is a direct adverse effect on the heart, *versus* a centrally mediated event; it has the additional advantage of higher throughput, as compared to conducting CV studies with telemetered animals.

As shown in Table 3, a remarkable difference in the activity of chromenes **30**/**32** and cyclopropyl chromanes **44**/**45** was

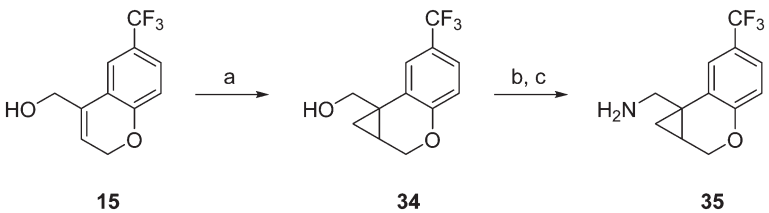

Scheme 7 First-generation synthesis of cyclopropyl chromane amines. Reagents and conditions: (a) $ZnEt_2$, CH_2I_2, 88%; (b) CBr_4, PPh_3, 70%; (c) NH_3/MeOH, 93%.

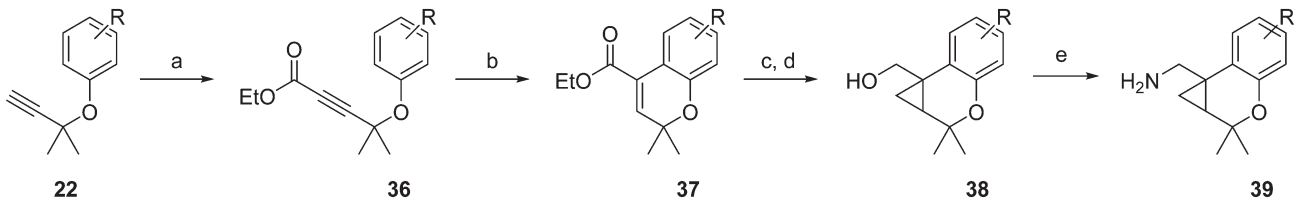

Scheme 8 Second-generation synthesis of cyclopropyl chromane amines. Reagents and conditions: (a) *n*-BuLi, −78 °C, then ethyl chloroformate; (b) (JohnPhos)Au(MeCN)SbF_6 (1–5 mol%); (c) trimethylsulfoxonium iodide, *t*-BuOK; (d) DIBAL-H; (e) Ts_2O, NEt_3, then 7 N NH_3/MeOH. Note: R = Cl, CF_3, OCF_3, OMe; see Table 2 for details.

Table 2 *In vitro* pharmacology and disposition data for cyclopropyl pyridopyrazine-1,6-dione GSMs **33–45**

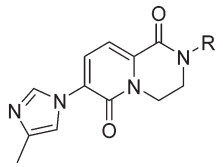

	R	IC_{50} (Aβ42, nM)[a]	clog *P*	MDR ER[b]	HLM $CL_{int,app}$ (μL/min/mg)[c]
33	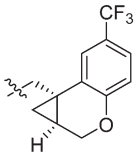	5.6	2.2	2.4	37.9
40	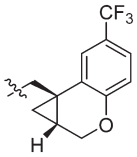	129	2.2	1.9	70.5
41	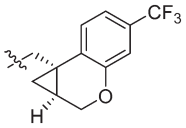	52	2.2	1.7	14.6
42	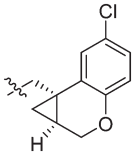	63	1.9	1.8	43.9
43	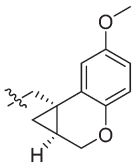	181	1.2	2.2	33.7
44	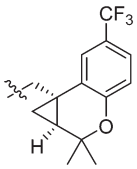	4.9	3.2	2.5	34.5
45	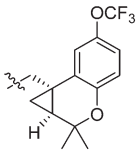	5.1	3.3	2.1	42.4

[a] Aβ42 IC_{50} values were obtained in a whole-cell assay using CHO APP_{wt} cells. Aβ42 IC_{50} values are the geometric mean of at least three experiments. [b] MDR efflux ratio using an MDR1/MDCK assay utilizing MDCK cells transfected with the gene that encodes human P-glycoprotein.[27] [c] Human liver microsome-derived intrinsic clearance.[22,23]

observed in the Langendorff assay. Chromenes **30** and **32** exhibited potent and rapid effects on left ventricular pressure/contractility and perfusion pressure, whereas the corresponding cyclopropyl chromanes **44** and **45** were devoid of activity against these endpoints at concentrations >30 μM. The chromenes completely inhibited left ventricular contractility in this preparation while dramatically increasing coronary perfusion pressure. These results supported the hypothesis that the observed lethality may be attributed to a CV-mediated adverse event. Rat dose-escalation studies were subsequently conducted with all four lead compounds to establish translation from the Langendorff assay to *in vivo* tolerability. As indicated in Table 3, lethality was observed with both chromenes **30** and **32**, at 30 mg kg^{-1} and 100 mg kg^{-1}, respectively, whereas the corresponding cyclopropyl chromanes **44** and **45** exhibited excellent tolerability up to

and including a 300 mg kg^{-1} dose. The *in vivo* findings observed with the chromenes **30** and **32** occurred at unbound C_{max} exposures of 205 nM and 620 nM, respectively. A similar rank order of potency was observed in the Langendorff assay, where effects on contractility were observed, albeit with IC_{50} values that were approximately 4.0 to 6.6-fold higher (IC_{50} values of 1355 nM and 2477 nM for **30** and **32**, respectively). It is interesting to note that this relatively small structural modification (replacement of an olefin with a cyclopropyl ring and removal of the chiral methyl group) had such a dramatic impact on cardiovascular safety. Notably, the specific target responsible for this effect was not identified, in spite of broad off-target pharmacology screening at Cerep. The Langendorff assay served as an efficient phenotypic counter-screen; it was subsequently used prospectively in the screening funnel to prioritize compounds for advancement.

Having established that the cyclopropyl chromane series was devoid of activity in the Langendorff assay while exhibiting excellent tolerability in rat dose-escalation studies at 300 mg kg^{-1}, this series was selected for further profiling *in vitro* and *in vivo*. Compound **44** exhibited the best overall profile; key *in vitro* and *in vivo* data is given in Table 4. Excellent selectivity was achieved over notch (notch intracellular domain, NICD)[31] and hERG[32] (>3200-fold and 3180-fold, respectively), while acceptable physicochemical properties were maintained. As noted earlier, the lead series was specifically designed to target moderate lipophilicity space, given the suboptimal *in vitro*/*in vivo* correlation that had been observed with earlier, more polar compounds in similar *in vitro* potency space. Nevertheless, compound **44** demonstrated favorable *in vitro* ADME characteristics, including good microsomal stability and passive permeability and adequate MDR efflux ratio (HLM $CL_{int,app}$ = 34.5 μL/min/mg, RRCK $P_{app,\ A\rightarrow B}$ = 5.3 × 10^{-6} cm s^{-1},[33] MDR ER = 2.5). This, in turn, resulted in an encouraging rat pharmacokinetic profile (CL = 26.4 mL/min/kg, F = 67%) and acceptable rodent brain penetration as indicated by an unbound brain-to-plasma ratio ($C_{b,u}/C_{p,u}$) of 0.23.

Compound **44** was examined in rat time-course studies at oral doses of 10 and 40 mg kg^{-1} to assess its effect on *de novo* synthesis of brain Aβ42. As shown in Fig. 3, robust, dose- and time-dependent reductions were achieved as compared to vehicle treatment, and at the 4 h time-point, the levels of brain Aβ42 were maximally reduced by 40% and 62% at the 10 mg kg^{-1} and 40 mg kg^{-1} dose, respectively. The corresponding unbound brain concentrations at this time-point were 11 and 67 nM for the two doses, respectively (see ESI† for details on Aβ42 reductions at each time point and the corresponding brain and plasma exposure). Notably, the robust central efficacy of **44** was achieved at a significantly lower dose and with reduced unbound brain drug concentrations as compared to earlier GSMs such as **3**. Compound **3** required an unbound brain concentration of 225 nM to afford a 40% maximal reduction of brain Aβ42 at the 3 h time-point.[17,37] Compound **44**, on the other hand, achieved the same level of Aβ42 reduction at an unbound brain drug level of only 11 nM, despite similar *in vitro* IC_{50} values for these two compounds. The significantly improved *in vivo* efficacy of **44** relative to earlier compounds, in concert with its maintaining a favorable physicochemical property profile and overcoming the safety hurdles observed in the rat dose-escalation studies, marked an important milestone for the program.

Table 3 Correlation between activity in the Langendorff assay and *in vivo* toleration studies in rats

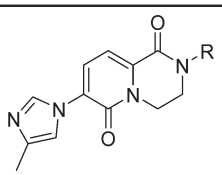

R Compound	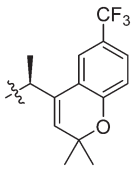 **30**	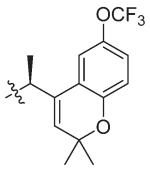 **32**	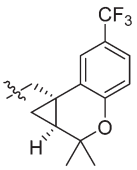 **44**	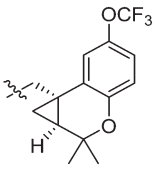 **45**
Aβ42 (IC_{50}, nM)	4.9	6.0	4.9	5.1
Contractility (IC_{50}, nM)	1355	2477	>30 000	>30 000
Left ventricle pressure (IC_{50}, nM)	1031	1625	>30 000	>30 000
Perfusion pressure (EC_{50}, nM)	576	1369	>30 000	>30 000
Observation/dose in rat dose-escalation study	Lethality (1/6)[a] at 30 mg kg^{-1}	Lethality (1/6)[b] at 100 mg kg^{-1}	Well tolerated at 300 mg kg^{-1}	Well tolerated at 300 mg kg^{-1}
C_{max} at indicated dose	5.84 μM total 205 nM free	17.7 μM total 620 nM free	90.4 μM total 1620 nM free	60.9 μM total 670 nM free

[a] Observed with 1/6 rats when dosed at 30 mg kg^{-1} p.o. and 6/6 rats when dosed at 100 mg kg^{-1} p.o. [b] Observed with 1/6 rats when dosed at 100 mg kg^{-1} p.o. (highest dose for this compound).

Table 4 *In vitro* and *in vivo* profile of compound **44**

Parameter	Measurement
In vitro potency/selectivity	
Aβ42 (IC_{50}, nM)	4.9
NICD (IC_{50}, μM)	>15.8
hERG (IC_{50}, μM)	15.6
Physicochemical properties	
clog *P*/log *D*[a]	3.2/3.8
LipE/LipMetE	4.5/1.5
CNS MPO[b]	3.9
Solubility (pH 6.5)[c]	63 μM
In vitro ADME	
HLM $CL_{int,app}$	34.5 μL/min/mg
RRCK $P_{app,\ A\rightarrow B}$	5.3×10^{-6} cm s^{-1}
MDR ER	2.5
CYP 1A2 IC_{50}	>30 μM
CYP 2C19 IC_{50}	16.9 μM
CYP 2C8 IC_{50}	7.2 μM
CYP 2C9 IC_{50}	22.7 μM
CYP 2D6 IC_{50}	14.2 μM
CYP 3A4 IC_{50}	16.3 μM
Rat PK profile	
CL[d]	26.4 mL/min/kg
$T_{1/2}$[d]	1.6 h
%*F*[e]	67%
B/*P*[f]	0.76
$C_{b,u}/C_{p,u}$[g]	0.23

[a] Shake flask log *D*.[34] [b] Calculated CNS MPO desirability score was obtained using the published algorithm.[35] [c] Kinetic solubility was measured at Analiza Inc.[36] [d] Determined from 1 mg kg^{-1} intravenous dose. [e] Determined from 1 mg kg^{-1} intravenous dose and 5 mg kg^{-1} oral dose. [f] Determined from the brain and plasma exposure at the 1, 2, 4, and 7 h time-points following a 5 mg kg^{-1} subcutaneous dose. [g] Plasma and brain free fractions of **44** in rat were 1.8% and 0.54%, respectively.

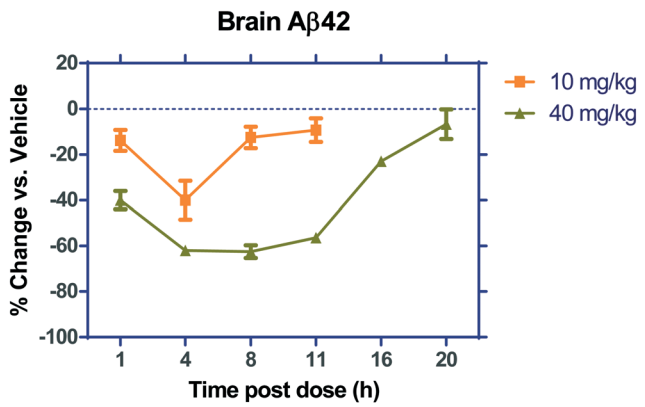

Fig. 3 Rat *in vivo* efficacy of cyclopropyl chromane **44**.

Conclusion

Herein we have described the design and synthesis of a novel series of GSMs that incorporate chromene- and cyclopropyl chromane-derived heterocyclic systems as bioisosteres for a naphthyl moiety that was present in preliminary lead **4**. Molecular modeling played a key role in rationalizing the 3D conformation of the series and subsequently evaluating and prioritizing new design ideas. The observation of apparent C_{max}-driven lethality in subsequent *in vivo* rat efficacy studies led to the hypothesis that chromenes **30** and **32** may carry a CV liability. This prompted the use of the Langendorff isolated heart model to examine a potentially direct CV effect on the heart. Chromenes **30** and **32** displayed dose-dependent effects on left ventricular pressure/contractility and perfusion pressure, whereas compounds in the closely related cyclopropyl chromane series (**44** and **45**) were devoid of activity in the Langendorff assay. This translated into excellent tolerability up to 300 mg kg^{-1} in rat dose-escalation studies with **44** and **45**. Taken together, these studies highlight how subtle structural modifications can have a profound effect on the safety profile of a given series. Lead cyclopropyl chromane **44** demonstrated excellent *in vitro* potency (Aβ42 IC_{50} = 4.9 nM) while maintaining acceptable lipophilicity (clog *P* = 3.2) and ADME parameters. This led to robust and sustained reductions of brain Aβ42 in rat time-course studies when dosed orally at 10 and 40 mg kg^{-1}. *In vivo* efficacy of **44** was achieved at significantly lower doses and free drug levels relative to earlier compounds such as **3** thus meeting a key design objective. In conclusion, the overall profile of **44** supports further advancement and in-depth characterization of its *in vivo* efficacy and safety.

Experimental section

General information

All solvents and reagents were obtained from commercial sources and were used as received. Reactions were monitored by TLC (TLC plates F254, Merck) or UPLC-MS analysis (Waters Acquity, ESCI +/−, APCI +/−). Gas chromatography-mass spectrometry (GC-MS) was performed with an Agilent 5890 GC Oven and an Agilent 5973 Mass Selective Detector. Melting points were obtained with a Thomas-Hoover melting point apparatus and are uncorrected. ^{1}H NMR and ^{13}C NMR spectra were obtained using deuterated solvent on a Varian 400 MHz instrument. All ^{1}H NMR shifts are reported in δ units (ppm) relative to the signals for chloroform (7.27 ppm) and methanol (3.31 ppm). All ^{13}C shifts are reported in δ units (ppm) relative to the signals for chloroform (77.0 ppm) and methanol (49.1 ppm) with ^{1}H-decoupled observation. All coupling constants (*J* values) are reported in hertz (Hz). NMR abbreviations are as follows: br, broadened; s, singlet; d, doublet; t, triplet; q, quartet; p, pentuplet; m, multiplet; dd, doublet of doublets; ddd, doublet of doublet of doublets. High-resolution mass spectra (HRMS) were acquired on an Agilent model 6220 MS (TOF). Optical rotations were determined with a Jasco P-2000 polarimeter. Column chromatography was carried out on silica gel 60 (32–60 mesh, 60 Å) or on prepacked Biotage™ or ISCO columns. HPLC purity analysis of the final test compounds was carried out using one of five methods. Method A: UPLC/UV/MS using a Waters Acquity CSH C18 column, 2.1 × 50 mm, with 1.7 μm particles; UV purity detected at 215 nm; mass spectrometer ESI positive/

negative switching, acquiring from *m*/*z* 150 to 1000; mobile phase A = 0.1% formic acid in water (v/v); mobile phase B = 0.1% formic acid in acetonitrile (v/v); gradient beginning at 95% A, 5% B, increasing to 100% B over 1.2 min, and remaining at 100% B until 1.5 min; flow rate: 1.0 mL min^{-1}. Method B: column: Waters Atlantis dC18 4.6 × 50 mm, 5 μm; mobile phase A: 0.05% TFA in water (v/v); mobile phase B: 0.05% TFA in acetonitrile (v/v); gradient: 95.0% H_2O/5.0% acetonitrile, linear to 5% H_2O/95% acetonitrile in 4.0 min, HOLD at 5% H_2O/95% acetonitrile to 5.0 min. Flow rate: 2 mL min^{-1}. Purity detected at 215 nm. Mass spectrometer ESI positive acquiring from *m*/*z* 160 to 2000 Da. Method C: UPLC/UV. Chembiotek Research International, Kolkata, India. Column: Agilent Zorbax SB C18, 50 × 4.6 mm, 1.8 μm; UV purity detected at 220 nm; mobile phase A = 0.05% TFA in water; mobile phase B = acetonitrile. Method D: UPLC/UV. Chembiotek Research International, Kolkata, India. Column: Waters Atlantis dC18, 50 × 4.6 mm, 1.8 μm; UV purity detected at 220 nm; mobile phase A = 0.05% TFA in water; mobile phase B = acetonitrile. Method E: UPLC/UV/MS using Chiral Technologies CHIRALPAK® AS-H column, 4.6 × 100 mm, 5 μm; mass spectrometer ESI positive, acquiring from *m*/*z* 160 to 650; mobile phase A = CO_2; mobile phase B = methanol; 80 : 20 A/B hold for 10 min; column temperature: 40 °C; back pressure: 120 Bar; flow rate: 1.5 mL min^{-1}. All final compounds were determined to have a purity of >95% by one of the aforementioned methods unless stated otherwise.

Synthesis of 2-{[(1a*S*,7b*S*)-2,2-dimethyl-6-(trifluoromethyl)-1*a*,2-dihydrocyclopropa[*c*]chromen-7b(1*H*)-yl]methyl}-7-(4-methyl-1*H*-imidazol-1-yl)-3,4-dihydro-2*H*-pyrido[1,2-*a*]-pyrazine-1,6-dione (44)

N-{[2,2-Dimethyl-6-(trifluoromethyl)-1*a*,2-dihydrocyclopropa[*c*]chromen-7b(1*H*)-yl]methyl}-1-(2-hydroxyethyl)-5-(4-methyl-1*H*-imidazol-1-yl)-6-oxo-1,6-dihydropyridine-2-carboxamide. 1-[2,2-Dimethyl-6-(trifluoromethyl)-1*a*,2-dihydrocyclopropa[*c*]chromen-7b(1*H*)-yl]methanamine (see ESI†) (3.60 g, 13.3 mmol) was dissolved in THF (50 mL), and DABAL-Me_3 (97%, 4.5 g, 17 mmol) was added portion-wise. The reaction mixture was warmed to 45 °C for 45 min, whereupon lactone 7 (4.63 g, 18.9 mmol) was added. The resulting mixture was heated at reflux for 2 h, cooled in an ice bath and quenched *via* slow addition of water (10 mL). Aqueous 1 M NaOH solution (50 mL) was introduced and the mixture was stirred at room temperature for 15 min before being extracted with EtOAc. The combined organic layers were dried over Na_2SO_4, filtered, and concentrated under reduced pressure; the residue was suspended in diethyl ether and collected *via* filtration to afford the product as an off-white solid. Yield: 6.10 g, 11.8 mmol, 89%. LCMS *m*/*z* 517 $[M + H]^+$. ^1H NMR (400 MHz, CD_3OD) δ 8.16 (d, *J* = 1.3 Hz, 1H), 7.85 (br d, *J* = 2.0 Hz, 1H), 7.62 (d, *J* = 7.5 Hz, 1H), 7.37 (ddq, *J* = 8.4, 2.2, 0.7 Hz, 1H), 7.21–7.23 (m, 1H), 6.86–6.90 (m, 1H), 6.37 (d, *J* = 7.5 Hz, 1H), 4.32–4.39 (m, 3H), 3.72–3.82 (m, 2H), 2.22 (d, *J* = 1.0 Hz, 3H), 1.90 (dd, *J* = 8.6, 5.9 Hz, 1H), 1.50 (s, 3H), 1.23 (s, 3H), 1.18 (dd, *J* = 8.7, 4.9 Hz, 1H), 1.07 (dd, *J* = 5.7, 5.1 Hz, 1H).

rel-2-{[(1a*S*,7b*S*)-2,2-Dimethyl-6-(trifluoromethyl)-1*a*,2-dihydrocyclopropa[*c*]chromen-7*b*(1*H*)-yl]methyl}-7-(4-methyl-1*H*-imidazol-1-yl)-3,4-dihydro-2*H*-pyrido[1,2-*a*]pyrazine-1,6-dione. Triethylamine (2.5 mL, 18 mmol) was added to a 0 °C suspension of *N*-{[2,2-dimethyl-6-(trifluoromethyl)-1*a*,2-dihydrocyclopropa[*c*]chromen-7*b*(1*H*)-yl]methyl}-1-(2-hydroxyethyl)-5-(4-methyl-1*H*-imidazol-1-yl)-6-oxo-1,6-dihydropyridine-2-carboxamide (6.10 g, 11.8 mmol) in THF (100 mL). Methanesulfonic anhydride (2.5 g, 14 mmol) was then added portion-wise, and the reaction mixture was stirred under ice cooling for 45 min. Additional triethylamine (1 mL, 7 mmol) and methanesulfonic anhydride (1 g, 6 mmol) were introduced, and stirring was continued for 2 h. After addition of triethylamine (1 mL, 7 mmol) and methanesulfonic anhydride (0.5 g, 3 mmol) and a further 30 min of stirring, TBD (6.0 g, 42 mmol) was added and the reaction was allowed to continue for 30 min at 0 °C. Additional TBD (2 g, 14 mmol) was introduced, and after 30 min at 0 °C, another charge of TBD (3 g, 21 mmol) was added. After 30 min, the reaction mixture was partitioned between water (100 mL) and EtOAc (750 mL). The organic layer was washed with water (100 mL), dried over Na_2SO_4, filtered, and concentrated under reduced pressure. The resulting residue was purified by silica gel chromatography (gradient: 0% to 10% MeOH in CH_2Cl_2) which provided partially purified material (4.8 g); this was treated with diethyl ether (50 mL), warmed to reflux for 10 min, cooled to room temperature, and filtered to provide the racemic title compound as a pale yellow solid (3.5 g, 7.0 mmol, 59%). ^1H NMR (400 MHz, $CDCl_3$) δ 8.21 (d, *J* = 0.9 Hz, 1H), 7.74 (d, *J* = 1.8 Hz, 1H), 7.45 (d, *J* = 7.7 Hz, 1H), 7.33–7.37 (m, 1H), 7.30 (d, *J* = 7.8 Hz, 1H), 7.12 (br s, 1H), 6.86 (d, *J* = 8.6 Hz, 1H), 4.96 (d, *J* = 14.8 Hz, 1H), 4.35 (ddd, *J* = 14.3, 6.7, 4.0 Hz, 1H), 4.19 (ddd, *J* = 14.3, 8.1, 4.2 Hz, 1H), 3.64–3.79 (m, 2H), 3.20 (d, *J* = 14.7 Hz, 1H), 2.28 (s, 3H), 1.80 (dd, *J* = 8.7, 5.8 Hz, 1H), 1.53 (s, 3H), 1.27 (s, 3H), 1.17 (dd, *J* = 5.7, 5.4 Hz, 1H), 1.08 (dd, *J* = 8.8, 5.3 Hz, 1H). The racemate was separated into its enantiomers *via* supercritical fluid chromatography (column: Phenomenex Lux Cellulose-1, 250 × 21.2 mm, 5 μm; isocratic conditions: mobile phase A: 60% carbon dioxide; mobile phase B: 40% methanol + 0.2% ammonium hydroxide; detection 210 nm; flow: 80.0 mL min^{-1}; back pressure: 120 Bar).

2-{[(1a*S*,7b*S*)-2,2-Dimethyl-6-(trifluoromethyl)-1*a*,2-dihydrocyclopropa[*c*]chromen-7*b*(1*H*)-yl]methyl}-7-(4-methyl-1*H*-imidazol-1-yl)-3,4-dihydro-2*H*-pyrido[1,2-*a*]pyrazine-1,6-dione (44). The first-eluting enantiomer (1.8 g) was suspended in ethyl acetate (25 mL), heated to reflux and treated with additional ethyl acetate (10 mL). After cooling to room temperature, a solid was removed *via* filtration, and the filtrate was concentrated under reduced pressure to provide an off-white solid. This was dissolved in ethyl acetate (10 mL), heated to reflux and treated with heptane (20 mL); the mixture was cooled to room temperature and the resulting crystalline solid was isolated *via* filtration and washed with heptane

(1.36 g, 2.73 mmol, 23%). m.p. 198–202 °C softens, 203–204 °C melts and decomposes; LCMS *m*/*z* 499.3 $[M + 1]^+$; ^{1}H NMR (400 MHz, CD_3OD) δ 8.27–8.28 (m, 1H), 7.86–7.89 (m, 1H), 7.77 (d, J = 7.8 Hz, 1H), 7.31–7.35 (m, 1H), 7.26–7.30 (m, 2H), 6.86 (d, J = 8.4 Hz, 1H), 5.17 (d, J = 14.8 Hz, 1H), 4.28–4.36 (m, 1H), 4.14–4.22 (m, 1H), 3.73–3.85 (m, 2H), 3.05 (d, J = 14.6 Hz, 1H), 2.23 (s, 3H), 2.05 (dd, J = 8.6, 5.9 Hz, 1H), 1.52 (s, 3H), 1.30 (s, 3H), 1.10 (dd, J = 8.6, 5.0 Hz, 1H), 1.06 (dd, J = 5.5, 5.4 Hz, 1H); ^{13}C NMR (100 MHz, CD_3OD) δ 160.0, 157.4, 155.6, 138.9, 138.1, 136.4, 131.1, 130.4, 128.4, 126.1 (q, $^1J_{CF}$ = 270.7 Hz), 125.1 (q, $^3J_{CF}$ = 3.7 Hz), 124.5 (q, $^2J_{CF}$ = 32.3 Hz), 124.4 (q, $^3J_{CF}$ = 3.7 Hz), 119.8, 116.6, 110.1, 73.8, 51.0, 45.2, 41.2, 35.8, 28.5, 26.6, 21.3, 16.0, 13.3; $[\alpha]_D^{22}$ −15.0 (*c* 0.99, MeOH); HRMS *m*/*z*, calcd $[M + H]^+$ for $C_{26}H_{25}F_3N_4O_3$ 499.1952, observed 499.1956; retention time: 8.35 minutes (column: Phenomenex Lux Cellulose-1, 4.6 × 250 mm, 5 μm; mobile phase A: carbon dioxide; mobile phase B: 0.2% [7 M solution of ammonia in ethanol] in methanol; gradient: 5% B from 0 to 1.0 minute, then linear from 5% to 60% B for 8.5 minutes; flow rate: 3.0 mL per minute). The indicated stereochemistry was assigned on the basis of single crystal X-ray determination of compound **44** (see ESI† for details).

2-{[(1a*R*,7b*R*)-2,2-dimethyl-6-(trifluoromethyl)-1*a*,2-dihydrocyclopropa[*c*]chromen-7*b*(1*H*)-yl]methyl}-7-(4-methyl-1*H*-imidazol-1-yl)-3,4-dihydro-2*H*-pyrido[1,2-*a*]pyrazine-1,6-dione (ent-44). The second-eluting enantiomer yielded the enantiomer of compound **44** (ent-**44**) (1.8 g, 3.6 mmol, 30%). LCMS *m*/*z* 499.3 $[M + H]^+$. ^{1}H NMR (400 MHz, CD_3OD) δ 8.27 (br s, 1H), 7.86–7.89 (m, 1H), 7.77 (d, J = 7.8 Hz, 1H), 7.31–7.35 (m, 1H), 7.26–7.30 (m, 2H), 6.86 (d, J = 8.6 Hz, 1H), 5.17 (d, J = 14.6 Hz, 1H), 4.28–4.36 (m, 1H), 4.14–4.22 (m, 1H), 3.73–3.85 (m, 2H), 3.05 (d, J = 14.6 Hz, 1H), 2.23 (s, 3H), 2.05 (dd, J = 8.5, 6.0 Hz, 1H), 1.52 (s, 3H), 1.30 (s, 3H), 1.04–1.13 (m, 2H). Retention time: 9.56 min, using conditions identical to those described above for compound **44**.

All animal experiments were carried out in strict accordance with federal, state, local and institutional guidelines governing the use of laboratory animals in research and were reviewed and approved by Pfizer Institutional Animal Care and Use Committee.

Abbreviations used

Aβ	Amyloid-β peptide
AD	Alzheimer's disease
ADME	Absorption, distribution, metabolism, and excretion
APP	Amyloid precursor protein
AB	Apical to basolateral
BA	Basolateral to apical
$CL_{int,app}$	Apparent intrinsic clearance
CNS MPO	Central nervous system multiparameter optimization
CSF	Cerebrospinal fluid
CV	Cardiovascular
CYP	Cytochrome P450
GSI	γ-Secretase inhibitor
GSM	γ-Secretase modulator
HHEP	Human hepatocytes
HLM	Human liver microsomes
LipE	Lipophilic efficiency
LipMetE	Lipophilic metabolism efficiency
MDCK	Madin–Darby canine kidney
MDR1	Multidrug resistance protein (P-glycoprotein, P-gp)
PK	Pharmacokinetic
PD	Pharmacodynamic
PS	Presenilin
RLM	Rat liver microsomes
SAR	Structure–activity relationship
TPSA	Topological polar surface area

Acknowledgements

We thank Stacey Becker, Emily Miller, Michael Marconi, Emily Sylvain, Don Tyszkicwicz, and Karin Wallace for their contributions to the *in vivo* studies. We also thank the Pfizer ADME technology group for generating the *in vitro* pharmacokinetic data to support the SAR efforts and Scott Obach and Loretta Cox for metabolite ID studies. We would like to thank Qingli Zhang and her team at WuXi Apptec and Sajal Mal at Chembiotek for synthetic contributions. Finally we thank Brian Samas for X-ray crystallographic analysis and Katherine Brighty for critical review of the manuscript.

References

1 W. Thies and L. Bleiler, 2013 Alzheimer's disease facts and figures, *Alzheimer's Dementia*, 2013, **9**, 208–245.
2 E. Karran, M. Mercken and B. De Strooper, The amyloid cascade hypothesis for Alzheimer's disease: an appraisal for the development of therapeutics, *Nat. Rev. Drug Discovery*, 2011, **10**, 698–712.
3 S. Weggen, J. L. Eriksen, P. Das, S. A. Sagi, R. Wang, C. U. Pietrzik, K. A. Findlay, T. E. Smith, M. P. Murphy, T. Bulter, D. E. Kang, N. Marquez-Sterling, T. E. Golde and E. H. Koo, A subset of NSAIDs lower amyloidogenic Aβ42 independently of cyclooxygenase activity, *Nature*, 2001, **414**, 212–216.
4 M. Z. Kounnas, A. M. Danks, S. Cheng, C. Tyree, E. Ackerman, X. Zhang, K. Ahn, P. Nguyen, D. Comer, L. Mao, C. Yu, D. Pleynet, P. J. Digregorio, G. Velicelebi, K. A. Stauderman, W. T. Comer, W. C. Mobley, Y.-M. Li, S. S. Sisodia, R. E. Tanzi and S. L. Wagner, Modulation of γ-secretase reduces β-amyloid deposition in a transgenic mouse model of Alzheimer's disease, *Neuron*, 2010, **67**, 769–780.
5 M. M. Murray, S. L. Bernstein, V. Nyugen, M. M. Condron, D. B. Teplow and M. T. Bowers, Amyloid beta protein: Aβ40 inhibits Aβ42 oligomerization, *J. Am. Chem. Soc.*, 2009, **131**, 6316–6317.
6 B. De Strooper, Lessons from a failed γ-secretase Alzheimer trial, *Cell*, 2014, **159**, 721–726.

7 V. Coric, C. H. van Dyck, S. Salloway, N. Andreasen, M. Brody, R. W. Richter, H. Soininen, S. Thein, T. Shiovitz, G. Pilcher, S. Colby, L. Rollin, R. Dockens, C. Pachai, E. Portelius, U. Andreasson, K. Blennow, H. Soares, C. Albright, H. H. Feldman and R. M. Berman, Safety and tolerability of the γ-secretase inhibitor avagacestat in a phase 2 study of mild to moderate Alzheimer disease, *Arch. Neurol.*, 2012, **69**, 1430–1440.

8 B. De Strooper, T. Iwatsubo and M. S. Wolfe, Presenilins and γ-secretase: structure, function, and role in Alzheimer disease, *Cold Spring Harbor Perspect. Med.*, 2012, **2**, a006304.

9 N. Pozdnyakov, H. E. Murrey, C. J. Crump, M. Pettersson, T. E. Ballard, C. W. am Ende, K. Ahn, Y.-M. Li, K. R. Bales and D. S. Johnson, γ-Secretase modulator (GSM) photoaffinity probes reveal distinct allosteric binding sites on presenilin, *J. Biol. Chem.*, 2013, **288**, 9710–9720.

10 C. J. Crump, D. S. Johnson and Y.-M. Li, Development and mechanism of γ-secretase modulators for Alzheimer's disease, *Biochemistry*, 2013, **52**, 3197–3216 and references therein.

11 M. Pettersson, A. F. Stepan, G. W. Kauffman and D. S. Johnson, Novel γ-secretase modulators for the treatment of Alzheimer's disease: a review focusing on patents from 2010 to 2012, *Expert Opin. Ther. Pat.*, 2013, **23**, 1349–1366.

12 H. J. M. Gijsen and M. Mercken, γ-Secretase modulators: can we combine potency with safety?, *Int. J. Alzheimer's Dis.*, 2012, **2012**, 295207.

13 M. Pettersson, D. S. Johnson, C. Subramanyam, K. R. Bales, C. W. am Ende, B. A. Fish, M. E. Green, G. W. Kauffman, R. Lira, P. B. Mullins, T. Navaratnam, S. M. Sakya, C. M. Stiff, T. P. Tran, B. C. Vetelino, L. Xie, L. Zhang, L. R. Pustilnik, K. M. Wood and C. J. O'Donnell, Design and synthesis of dihydrobenzofuran amides as orally bioavailable, centrally active γ-secretase modulators, *Bioorg. Med. Chem. Lett.*, 2012, **22**, 2906–2911.

14 For similar approaches, see A. Hall and T. R. Patel, γ-Secretase modulators: current status and future directions, *Prog. Med. Chem.*, 2014, **53**, 101–145, and references therein.

15 M. Pettersson, D. S. Johnson, C. Subramanyam, K. R. Bales, C. W. Am Ende, B. A. Fish, M. E. Green, G. W. Kauffman, P. B. Mullins, T. Navaratnam, S. M. Sakya, C. M. Stiff, T. P. Tran, L. Xie, L. Zhang, L. R. Pustilnik, B. C. Vetelino, K. M. Wood, N. Pozdnyakov, P. R. Verhoest and C. J. O'Donnell, Design, synthesis, and pharmacological evaluation of a novel series of pyridopyrazine-1,6-dione γ-secretase modulators, *J. Med. Chem.*, 2014, **57**, 1046–1062.

16 M. Pettersson, D. S. Johnson, J. M. Humphrey, T. W. Butler, C. W. am Ende, B. A. Fish, M. E. Green, G. W. Kauffman, P. B. Mullins, C. J. O'Donnell, A. F. Stepan, C. M. Stiff, C. Subramanyam, T. P. Tran, B. C. Vetelino, E. Yang, L. Xie, K. R. Bales, L. R. Pustilnik, S. J. Steyn, K. M. Wood and P. R. Verhoest, Design of pyridopyrazine-1,6-dione γ-secretase modulators that align potency, MDR efflux ratio, and metabolic stability, *ACS Med. Chem. Lett.*, 2015, **6**, 596–601.

17 M. Pettersson, D. S. Johnson, J. M. Humphrey, C. W. am Ende, E. Evrard, I. Efremov, G. W. Kauffman, A. F. Stepan, C. M. Stiff, L. Xie, K. R. Bales, E. Hajos-Korcsok, H. E. Murrey, L. R. Pustilnik, S. J. Steyn, K. M. Wood and P. R. Verhoest, Discovery of indole-derived pyridopyrazine-1,6-dione γ-secretase modulators that target presenilin, *Bioorg. Med. Chem. Lett.*, 2015, **25**, 908–913.

18 T. P. Tran, P. B. Mullins, C. W. am Ende and M. Pettersson, Synthesis of pyridopyrazine-1,6-diones from 6-hydroxypicolinic acids via a one-pot coupling/cyclization reaction, *Org. Lett.*, 2013, **15**, 642–645.

19 Values for clogP were calculated using the BIOBYTE (www.biobyte.com) program clogP, version 4.3.

20 W.-W. Qiu, K. Surendra, L. Yin and E. J. Corey, Selective formation of six-membered oxa- and carbocycles by the In(III)-activated ring closure of acetylenic substrates, *Org. Lett.*, 2011, **13**, 5893–5895.

21 R. S. Menon, A. D. Findlay, A. C. Bissember and M. G. Banwell, The Au(I)-catalyzed intramolecular hydroarylation of terminal alkynes under mild conditions: application to the synthesis of 2H-chromenes, coumarins, benzofurans, and dihydroquinolines, *J. Org. Chem.*, 2009, **74**, 8901–8903.

22 Assay method adapted from published protocols: R. J. Riley, D. F. McGinnity and R. P. Austin, A unified model for predicting human hepatic, metabolic clearance from in vitro intrinsic clearance data in hepatocytes and microsomes, *Drug Metab. Dispos.*, 2005, **33**, 1304–1311.

23 R. S. Obach, Prediction of human clearance of twenty-nine drugs from hepatic microsomal intrinsic clearance data: An examination of in vitro half-life approach and nonspecific binding to microsomes, *Drug Metab. Dispos.*, 1999, **27**, 1350–1359.

24 S. Ou, M. Jiang and J.-T. Liu, Synthesis of 2,2-difluoro-2H-chromenes through the tandem reaction of ethyl 3-bromo-3,3-difluoropropionate with salicylaldehyde derivatives, *Tetrahedron*, 2013, **69**, 10820–10825.

25 R. Pratap and V. J. Ram, Natural and synthetic chromenes, fused chromenes, and versatility of dihydrobenzo[h]chromenes in organic synthesis, *Chem. Rev.*, 2014, **114**, 10476–10526.

26 LipMetE was calculated using measured shake flask logD^{34} and unbound intrinsic clearance ($CL_{int,u}$) derived from the intrinsic apparent clearance ($CL_{int,app}$) and calculated human liver microsomal binding values. For additional detail, see A. F. Stepan, G. W. Kauffman, C. E. Keefer, P. R. Verhoest and M. Edwards, Evaluating the differences in cycloalkyl ether metabolism using the design parameter "lipophilic metabolism efficiency" (LipMetE) and a matched molecular pairs analysis, *J. Med. Chem.*, 2013, **56**, 6985–6990.

27 B. Feng, J. B. Mills, R. E. Davidson, R. J. Mireles, J. S. Janiszewski, M. D. Troutman and S. M. de Morais, *In vitro* P-glycoprotein assays to predict the *in vivo* interactions of P-glycoprotein with drugs in the central nervous system, *Drug Metab. Dispos.*, 2008, **36**, 268–275.

28 LipE = $-\log(EC_{50}) - \log D$ where EC_{50} is in molar units and $\log D$ was experimentally determined using shake flask log D.[33] For additional detail, see T. Ryckmans, M. P. Edwards, V. A. Horne, A. M. Correia, D. R. Owen, L. R. Thompson, I.

Tran, M. F. Tutt and T. Young, Rapid assessment of a novel series of selective CB_2 agonists using parallel synthesis protocols: A Lipophilic Efficiency (LipE) analysis, *Bioorg. Med. Chem. Lett.*, 2009, **19**, 4406–4409.

29 O. Langendorff, Geschichtliche betrachtungen zur methode des überlebenden warmblüterherzens, *Muench. Med. Wochenschr.*, 1903, **50**, 508–509.

30 M. Skrzypiec-Spring, B. Grotthus, A. Szelag and R. Schulz, Isolated heart perfusion according to Langendorff - Still viable in the new millennium, *J. Pharmacol. Toxicol. Methods*, 2007, **55**, 113–126.

31 Inhibition of notch signaling was determined by measuring notch intracellular domain (NICD) in inhibition of HEK 293 NdeltaE cells. See A. F. Stepan, K. Karki, W. S. McDonald, P. H. Dorff, J. K. Dutra, K. J. Dirico, A. Won, C. Subramanyam, I. V. Efremov, C. J. O'Donnell, C. E. Nolan, S. L. Becker, L. R. Pustilnik, B. Sneed, H. Sun, Y. Lu, A. E. Robshaw, D. Riddell, T. J. O'Sullivan, E. Sibley, S. Capetta, K. Atchison, A. J. Hallgren, E. Miller, A. Wood and R. S. Obach, Metabolism-directed design of oxetane-containing arylsulfonamide derivatives as γ-secretase inhibitors, *J. Med. Chem.*, 2011, **54**, 7772–7783.

32 J. Kutchinsky, S. Friis, M. Asmild, R. Taboryski, S. Pedersen, R. K. Vestergaard, R. B. Jacobsen, K. Krzywkowski, R. L. Schrøder, T. Ljungstrøm, N. Hélix, C. B. Sørensen, M. Bech and N. J. Willumsen, Characterization of potassium channel modulators with QPatch automated patch-clamp technology: system characteristics and performance, *Assay Drug Dev. Technol.*, 2003, **1**, 685–693.

33 E. Callegari, B. Malhotra, P. J. Bungay, R. Webster, K. S. Fenner, S. Kempshall, J. L. LaPerle, M. C. Michel and G. G. Kay, A comprehensive non-clinical evaluation of the CNS penetration potential of antimuscarinic agents for the treatment of overactive bladder, *Br. J. Clin. Pharmacol.*, 2011, **72**, 235–246.

34 Shake flask logD. Assay method adapted from published protocol: T. Hay, R. Jones, K. Beaumont and M. Kemp, Modulation of the partition coefficient between octanol and buffer at pH 7.4 and pK_a to achieve the optimum balance of blood clearance and volume of distribution for a series of tetrahydropyran histamine type 3 receptor antagonists, *Drug Metab. Dispos.*, 2009, **37**, 1864–1870.

35 T. T. Wager, X. Hou, P. R. Verhoest and A. Villalobos, Moving beyond rules: the development of a central nervous system multiparameter optimization (CNS MPO) approach to enable alignment of druglike properties, *ACS Chem. Neurosci.*, 2010, **1**, 435–449.

36 Analiza, Inc., Cleveland, OH. (http://analiza.com/physchem/logd.html#qf).

37 This experiment was conducted in guinea pig.

